Journal of Power Sources 267 (2014) 347–355

Contents lists available at ScienceDirect

Journal of Power Sources

journal homepage: www.elsevier.com/locate/jpowsour

Hybrid phosphazene anodes for energy storage applications

Eric J. Dufek*, Mark L. Stone, David K. Jamison, Frederick F. Stewart, Kevin L. Gering, Lucia M. Petkovic, Aaron D. Wilson, Mason K. Harrup, Harry W. Rollins

Idaho National Laboratory, P.O. Box 1625, Idaho Falls, ID 83415, USA

HIGHLIGHTS

- Hybrid cyclic phosphazene/graphite anodes are new materials for lithium batteries.
- Capacity resides with both the graphite and cyclic phosphazene.
- Within the cyclic phosphazene matrix isolated Li deposits are the main source of capacity.
- Tightly controlling the charging voltage provides enhanced cycling efficiency.

ARTICLE INFO

Article history:
Received 4 February 2014
Received in revised form
1 May 2014
Accepted 20 May 2014
Available online 2 June 2014

Keywords:
Phosphazene
Anode
Battery
Hybrid system
Lithium ion battery

ABSTRACT

The use of hybrid cyclic phosphazene polymer/graphite anodes, where the phosphazene serves as distributed loci for Li deposition, has been investigated. Capacity within the hybrid system was found to occur reversibly in distinct regions. At the most positive voltages, above 0.06 V vs Li/Li^+, the capacity was associated mostly with Li^+ intercalation into graphite. In the most negative region, deposition of Li within the polymer was the predominate mechanism. A transitional region is inferred by the data whereby bulk aggregation or clustering of Li atoms occurs in proximity to the phosphazene sites that then serve as a template for more widespread population of Li within the anode at higher voltages, akin to a nucleation process. In full cells with a mixed oxide cathode, controlling the extent of Li deposition by limiting the charging voltage to 4.45 V enabled repeated cycling with no loss in capacity. Capacities as high as 183 mAh g^{-1} have been achieved for systems containing as little as 10% graphite while retaining coulombic efficiencies of 98% over 50 cycles. This level of cycling equates to the deposition of 7.4 Li per cyclic phosphazene.

1. Introduction

Recent, safety related events have been a key concern for the continued market entry of Li-ion batteries (LIBs). While safe for the majority of operating conditions, improper use, exposure to harsh conditions and the puncturing of cells can lead to catastrophic failure. Despite concerns with safety, electrification of the transportation fleet in the United States remains an emphasis. To meet the need for enhanced safety, a host of new materials have been proposed. An important class of compounds are those that, when included in LIB electrolyte, reduce the risk of fire [1–8]. Electrolyte additives can significantly reduce safety concerns, but during heating events the majority of the electrolyte can be vented from cells while leaving the highly combustible anode materials remaining within the LIB. Thus, a different route to increasing the safety of batteries is the use of non-flammable electrode components which remain present even after a venting event.

During LIB thermal events it has been found that the anode is one of the key players in the initiation of the catastrophic failure process [9]. In instances where heating occurs, the solid electrolyte interphase (SEI) on the anode becomes less stable leading to a cascade of reactions which expose lithiated and non-lithiated graphite surfaces. Both are active to the decomposition of electrolyte. Upon sufficient heating, cathodic oxygen generation causes oxidation of electrolyte and eventually the anode during a thermal runaway event [9–11]. In the events described above, materials, such as phosphazenes, that either decrease or inhibit the initiation events, or which minimize the amount of material which can be oxidized provide the opportunity to limit the extent of thermal events and thus enhance the safety of LIBs.

Phosphazenes are a class of inorganic compounds containing P═N bonds that have received some interest primarily as

* Corresponding author. Tel.: +1 208 526 2132; fax: +1 208 526 8541.
E-mail address: eric.dufek@inl.gov (E.J. Dufek).

http://dx.doi.org/10.1016/j.jpowsour.2014.05.105
0378-7753/

electrolyte additives, components in polymer electrolytes and to a lesser extent as binders [1,8,12–18]. One of the attractions of phosphazenes is their ability to act as flame retardants. Additional benefits of phosphazenes are their high adaptability which provides the opportunity to synthesize functionality into the overall molecular framework. This adaptability has led to the construction of both small cyclic phosphazenes which have been incorporated in electrolytes [1,18] and much larger linear polyphosphazene compounds which can act as effective ionic transporters [12–14,19,20]. Lastly, phosphazenes have shown electrochemical stability over a sufficiently large window to allow functionality in LIB systems [1,8,17,18].

One of the primary reasons for investigating the use of hybrid phosphazene anodes is the ability of phosphazenes to act as free-radical scavengers. Combustion can be viewed as a cascading radical pathway, thus the ability to stop the early stages of combustion are essential when trying to minimize the overall flammability of batteries. The use of solid-state cyclic phosphazenes as an anode component looks to build on the previous success of phosphazene electrolyte additives [1,8,18] to further enhance the safety of cells by providing the possibility of retaining the phosphazene in the vicinity of combustible carbon in the cell anode should electrolyte-based phosphazene be ejected during cell venting.

As electrode materials, only a few instances where phosphazenes have been used as cathodes have been reported [21,22]. These cathodes, while showing cyclability, suffer from the low reduction potential of the S–S bond which occurs below 3 V versus Li/Li^+. In another application as polymer-based electrolytes, phosphazenes have shown Li-ion conductivity values as high as 2.58×10^{-4} S cm^{-1} when employed as polymer based electrolytes [14]. Additionally, both experimental and modeling data for liquid electrolytes indicate an association of Li^+ with the O and N components of the phosphazene backbone [19,23]. In the case of N:Li^+ association, this electrostatic attraction is caused by the electron pair donation centered at N that responds to cationic fields. Such associative effects enable nitrogen-containing aprotic solvents to be very aggressive, competitive solvators of cations as indicated by their high donicity numbers [24]. Consequently, the association of Li with the polymer phosphazene moieties creates the situation where Li^+ are less

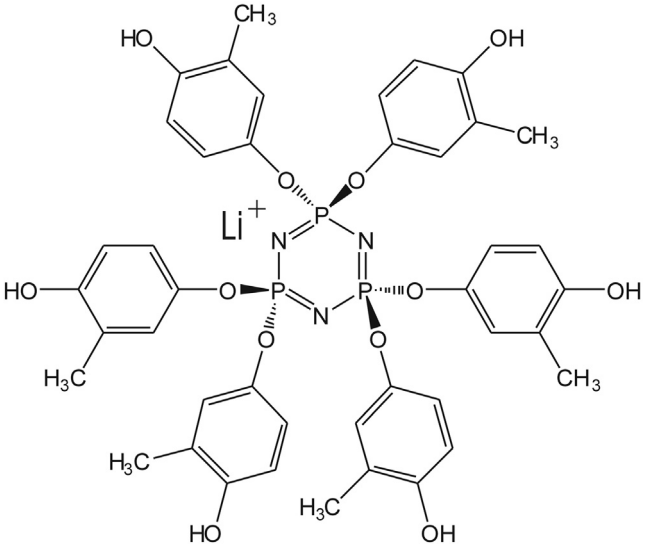

Fig. 1. Molecular structure of MeHQCP with the location of Li noted.

than fully solvated and as such when reduced to Li^0 the interaction with liquid electrolyte is minimized due to less electrolyte in the vicinity of the Li deposit. The N-based electron pair also serves to provide an electrostatic repulsion with the negative dipole of free solvents providing an additional short-range minimization of electrolyte near deposits of Li. Decreasing the electrolyte in contact with Li serves to increase the coulombic efficiency of hybrid electrodes by decreasing electrolyte decomposition. An additional side benefit is that hybrid phosphazene anodes may minimize the formation of dendrites by creating micro-clusters of Li in the electrode interior as has been recently reported for porous graphene electrodes [25]. When combined with traditional anode materials such as graphite, the use of solid-state phosphazenes provides a route to a hybrid Li-ion, Li-metal anode where the phosphazene serves as a template for selective, localized Li deposition which is isolated from the bulk electrolyte. Such a hybrid anode has the potential, if fully optimized, to be tunable with regard to capacity while retaining the safety enhancing aspects of phosphazene systems. A recent patent application covers this new class of materials [26].

2. Experimental

2.1. Anode film preparation

Cyclic phosphazenes were prepared using well established procedures with the primary compounds of interest being methyl hydroquinone cyclophosphazene (MeHQCP) and tert-butyl hydroquinone cyclophosphazene (tbu-HQCP) [27,28]. The structure for MeHQCP is shown in Fig. 1, as an example. Following synthesis, purity was confirmed by ^{1}H NMR.

Casting solutions were prepared, using a method developed in-house, by first dissolving the appropriate amount of phosphazene in tetrahydrofuran (THF, 10–15 mL) followed by the addition of varying quantities of C65 conductive carbon additive (Timcal), and A12 graphite (Conoco-Philips). An assortment of sample formulations is shown in Table 1. The solids and phosphazene solution was mixed by inversion and then sonicated to enhance homogeneity. Following sonication, 0.10–0.50 g of hexamethylene tetramine (HMTA) dissolved in 0.25–1.0 mL H_2O was added to the suspension. The quantity of HMTA added varied with the cyclic phosphazene loading. Following addition of HMTA, the casting solution was again mixed by inversion. The solution was then loaded into a chromatography sprayer and sprayed onto high purity Cu foil or polyimide sheets. During the spray casting process these substrates were fixed onto a vertically mounted, rotating wheel to ensure uniform coating over multiple substrates.

Spraying occurred in multiple steps where a portion of the solution was sprayed evenly on the substrate followed by a brief pause during which THF evaporated. The evaporation step ensured that the sprayed film did not flow during the casting process. During evaporation steps the casting solution in the sprayer was continuously swirled to maintain uniform dispersion of the solid particles. Following the last spray step, the coated substrates were removed and placed onto a clean, stainless steel sheet. The sheet was loaded into an oven (130 °C). During the curing step the temperature in the oven was ramped from 130 °C to 210 °C. The entire curing protocol took approximately 30 min to complete. The curing protocol served two purposes. First it allowed HMTA to decompose to formaldehyde which allows cross-linking of multiple rings through a phenol-formaldehyde mechanism. Second the temperature ramp served to fully evaporate any trace THF and H_2O which remained in the electrode. For each of the investigated formulations

Table 1
Anode specifications.

Formulation	Cyclic phosphazene	Cyclic phosphazene, %	A12, %	C65, %	Film thickness, μm	Entire electrode mass, mg	V_{max}, V	Capacity from A12,[c] mAh g^{-1}
1	MeHQCP	80	10	10	80 ± 3	6.60	4.65	37, 11
2	MeHQCP	80	10	10	80 ± 3	6.60	4.25[a]	37, 22
3	MeHQCP	65	25	10	82 ± 2	4.10	4.65	92, 16
4	MeHQCP	80	0	20	98 ± 7	8.23	4.65	0, na
5	tbuHQCP	80	0	20	105 ± 3	6.56	4.65	0, na
6	MeHQCP	10	80	10	91 ± 5	4.30	4.25[b]	296, 79

[a] Increased to 4.45 V after 29 cycles.
[b] Increased to 4.65 V after 16 cycles.
[c] Accounting for the entire formulated electrode mass, values after commas correspond to the percent of experimental discharge capacity associated with graphite after 10 cycles at the maximum voltage.

uniform films were formed on each of the substrates. For coin cell investigations films were formed on 18 μm Cu sheets which were nominally 2.5 cm in width and 25 cm in length. As shown in Table 1, the film thicknesses ranged from 80 to 105 μm with relative standard deviations for all the samples below 10%. Both MeHQCP and tbuHQCP in their non-crosslinked, trimeric forms are also soluble in the ethylene carbonate (EC), ethyl methyl carbonate (EMC) electrolyte blend used for the present study. Upon crosslinking with HMTA the new polymeric systems become insoluble.

2.2. Cell fabrication

The anode formulations were evaluated using CR 2032 coin cell hardware. Full cells were constructed using the formulations listed in Table 1 as the anode and a lithium-rich blended $Li_{1.06}Mn_{1.94}O_4$ + $Li_{1.1}Ni_{0.33}Mn_{0.33}Co_{0.33}O_2$ cathode (Argonne National Laboratory, ANL). The rated cathode capacity as defined by ANL is 3.47 mAh per electrode, or 2.43 mAh cm^{-2}. Extended cycling against an A12 anode (ANL) to 4.25 V maintained cell capacities above 3.1 mAh for more than 50 cycles. All cells used a 1:2 EC:EMC (Kishida) with 1.2 M $LiPF_6$ (Kishida). The electrolyte also included a 3% loading of FM-2 ($C_{12}H_{21}F_9N_3O_6P_3$) which is a liquid cyclic phosphazene similar to previously described cyclic phosphazene electrolyte additives [1,8,18,23]. The geometric area of each electrode was 1.43 cm^2. Electrodes were separated using a Celgard 2325 separator (1.58 cm^2). Cell components were dried overnight at 90 °C under vacuum prior to the construction of cells. Separators were dried overnight at 60 °C under vacuum. Cells were built under an Ar atmosphere in a glove box with water and oxygen content below 0.1 ppm. Both the anode and cathode were fully wetted with electrolyte to ensure uniform electrolyte distribution within each electrode prior to advancing to the next step in the cell build. Half-cells were constructed in a similar manner with Li metal serving as the counter electrode.

Stainless steel tabs were spot welded onto the positive and negative terminals of the cell prior to mounting in a custom cell holder. Within the holder, each cell was spaced a minimum of 5 cm from its nearest neighbor (with open space on all sides) and maintained in a horizontal orientation. The primary benefit of this orientation is uniform thermal profiles for each cell. Cell holders were maintained at 30 °C in a Tenney environmental chamber.

2.3. Electrochemical analysis and film characterization

All full cell formulations were evaluated in triplicate with cycling occurring at a calculated C/10 rate. Except where noted the average value from the three cells are shown. Prior to initiating testing, cells were allowed to equilibrate for 2 h after placement in the environmental chamber. A Maccor 4000 series test system which was calibrated prior to testing was used to cycle both full and half cells. Cells were initially taken through a staged formation cycle at a calculated C/10 rate where the charging voltage (V_{max}) was progressively increased by cycle. At the end of the formation protocol cells were cycled at a C/10 rate with a set V_{max} of 4.25, 4.45 or 4.65 V. The minimum voltage (V_{min}) was kept at 3.4 V for all full cell cycling. Half cells followed a similar protocol where the V_{min} was progressively lowered.

Scanning electron microscopy (SEM) imaging of electrode surfaces, both as formed and after cycling, was performed using a Quanta FEG 650 SEM. Images and energy dispersive spectra (EDS) were acquired from representative locations on the interior of the electrode. Cycled electrodes were harvested in an Ar glove box in a discharged state. After removal from the cell, both anode and cathode samples were briefly rinsed with dimethyl carbonate (DMC), allowed to dry and then removed from the glove box. Sheet resistance for each of the as-prepared formulations was acquired on the films sprayed onto the non-conductive polyimide using a four-point probe (Guardian SRM-232). Typical sheet resistances for the various formulations were 100–200 Ω sq^{-1}. Nitrogen physisorption isotherms were measured at 77 K on a Quantachrome Autosorb-1C system to determine the surface area of the various formulations. Sample pieces of about 2 cm^2 were rolled to fit into the instrument cell, outgassed at 383 K for 3 h, and weighed. The actual weight of the sample was calculated by subtracting the contribution of the metal foil to the weight measured after outgassing. Next the nitrogen physisorption isotherm was measured and used to calculate Brunauer-Emmett-Teller (BET) surface areas [29] in the P/P_0 range of 0.05–0.35 and both total pore volume and average pore size at $P/P_0 = 0.99$. Presence of microporosity was analyzed using the *t*-plot method [30].

3. Results and discussion

The use of linear polyphosphazenes as compounds capable of Li^+ transport has previously shown that ionic movement occurs along the backbone of the solid polymer with Li^+ interacting with both N and O atoms near the backbone of the polymeric chain [19]. This geometry is ideal for transporting Li ions such as what one would prefer when developing polymer electrolytes. However, one of the key proposed benefits of a hybrid anode system is the ability to form regions of Li which are isolated from the bulk liquid electrolyte. The anticipated location of Li, based on earlier characterization of linear systems using NMR, FTIR and Raman analysis [19] and based on modeling calculations of similar cyclic phosphazenes [23], for MeHQCP is shown in Fig. 1.

While retaining the beneficial Li interactions with N and O, as has been shown for the linear systems, the cyclic phosphazene systems have limited P═N connectivities (3 for the cyclic systems described) which promotes isolated Li association. Additionally the use of pendant arms such as the hydroquinones present for both MeHQCP and tbuHQCP provide spatial isolation which sterically limits the inter-electrode void space while still allowing extensive polymeric cross-linking through formaldehyde linkages at the hydroxyl terminus of the hydroquinone. Collectively, these attributes contribute to better managed lithium placement within the polymeric host. Lastly, the use of cyclic phosphazenes, which are soluble in a variety of solvents, enables casting methods such as spray casting which are amenable to the formation of unique electrode geometries. The assortment of formulations in serves to span the range from systems where the cyclic phosphazene serves solely as a binder within a more traditional anode formulation to the opposite extent where nearly the entire structure is comprised of cyclic phosphazene. For each of the formulations in the table, the anticipated specific capacity for the entire film which can be attributed to graphite is listed, i.e. the capacity derived from graphite divided by the entire film mass. The percentages listed after the comma in the same column highlight the percentage of the experimentally observed specific capacity after 10 cycles which would correspond with the full graphite capacity. For formulations 2 and 6 the percentages are for the capacity after the voltage was increased to 4.45 or 4.65 V respectively. As hybrid systems the anodes possess the ability to store charge through microclusters of Li deposits, similar to what has been recently reported for porous graphene systems [25], and in the portion of graphite within the anode. As such, some of the expected benefits associated with hybrid phosphazene anodes are the reduction in combustible material in the composite electrode, the inclusion of free-radical scavenging phosphazenes, and the potential to achieve capacities above what is achievable with graphite electrodes.

Prior to electrochemical evaluation of the anode films the films were characterized using SEM, surface area analysis and for electrical conductance. SEM imaging of the anode films, as shown in Fig. 2, indicate a dispersion of the various solid additives throughout the film. The images also show the presence of both large pores (Fig. 2A lower right) and much smaller porous regions located near the solid additives such as C65 and A12 in Fig. 2C. One of the key concerns of using electrode structures which incorporate a high quantity of polymeric material is adequate porosity and available surface area to allow electrolyte access to the interior of the electrode structure. BET analysis of the surface area and the total pore volume of prepared electrodes indicated that the values were comparable to more traditional electrode structures such as the cathode used in the present work. For comparison formulations **1** and **2** had a measured BET surface area of 11 $m^2\ g^{-1}$ with a total pore volume of $1.73 \times 10^{-2}\ cm^3\ g^{-1}$ (average pore diameter of 63 Å) while the calendared cathode had values 7 $m^2\ g^{-1}$, $1.32 \times 10^{-2}\ cm^3\ g^{-1}$ and 73 Å respectively.

Evaluation of the electrical conductance was performed on anode films which were cast on thin Kapton films at the same time as the deposition of films on Cu. The use of Kapton enabled the sheet resistance for just the phosphazene anode to be evaluated using a four point probe. For the six formulations reported the sheet resistances were between 100 and 200 $\Omega\ sq^{-1}$. For comparison other thin film battery electrodes have had reported sheet resistances between 10 and 30 $\Omega\ sq^{-1}$ [31,32]. While the present formulations have conductance values which exceed other electrodes a multitude of opportunities exist for decreasing the sheet

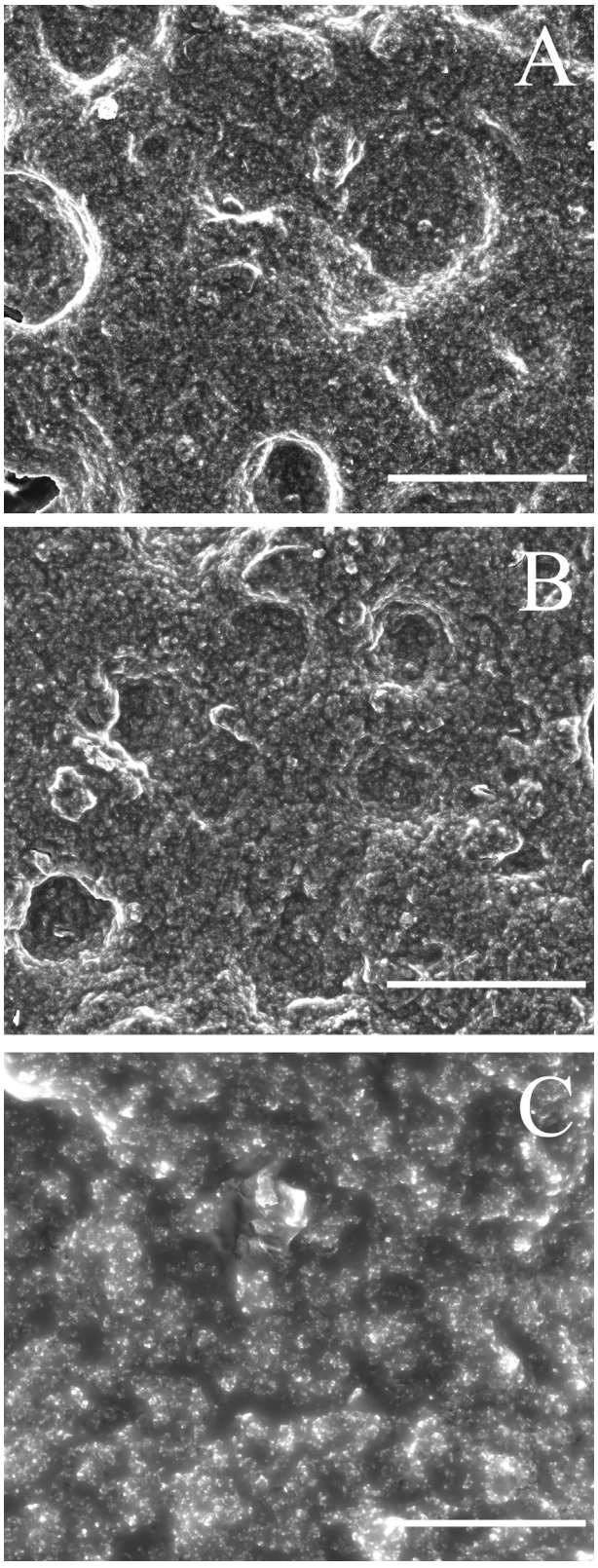

Fig. 2. SEM images for formulation **2** both before (A) and after cycling (B and C, after rinsing to remove electrolyte based salts). Scale bar represents 50 μm (A and B) or 10 μm (C).

resistances by further optimizing formulations, changing the nature of the conductive additive and by further modifying the phosphazene structure.

The respective full cell cycling data for the six formulations in Table 1 are shown in Fig. 3 where the specific capacities refer to the cell capacity divided by the respective mass of each of the formulations on the 1.43 cm^2 electrode. Full cells were chosen here to ensure compatibility between the anode and cathode. Testing was performed using the anode as the limiting electrode. During cycling the maximum observed discharge capacity for any of the phosphazene formulations was 2.71 mAh which is 78% of the rated capacity of the cathode and 87% of the capacity observed after 50 cycles using the present cathode coupled to a traditional graphite (A12) anode (data not shown). As shown in Fig. 3 the various formulations displayed high initial performance by the end of formation cycling (first 4–5 cycles depending on V_{max}). For cells which were cycled to 4.65 V, following formation, the behavior varied for the next 5–10 cycles before all experienced a loss in capacity. The extent and rate of capacity loss varied with respect to the formulation. However, for formulations **4** and **5** little difference was observed when using either tbuHQCP or MeHQCP as the cyclic phosphazene. For this reason the majority of future work focused on the use of MeHQCP which has a reduced molecular weight compared to tbuHQCP (873 vs 1125 g mol^{-1}).

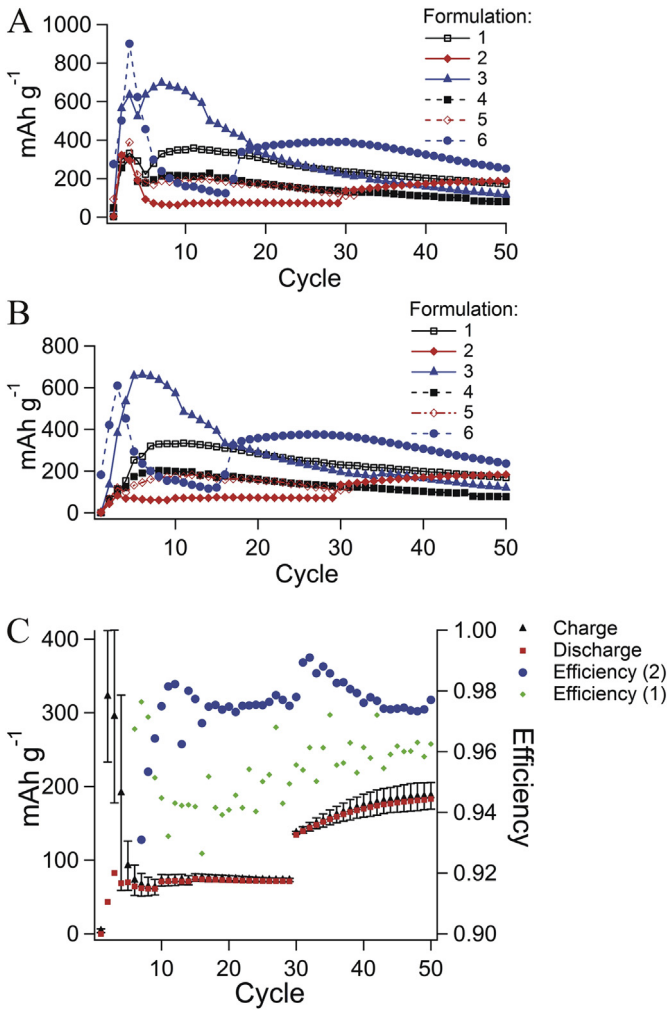

Fig. 3. Average charge (A) and discharge (B) capacities for formulations **1**–**6** at a C/10 rate. (C) Combined average charge and discharge profiles and corresponding coulombic efficiency for formulation **2**. Only charge standard deviations are shown for clarity. The standard deviations for the discharge values are on the order of those observed for charging.

For formulation **2**, which was initially cycled to 4.25 V the capacity remained constant with a slight increase in capacity over the first 25 cycles. Formulation **6**, which was also cycled initially to 4.25 V, initially showed a post formation capacity loss. After an increase in V_{max} to 4.65 V behavior similar to formulations **1** was observed. Based on the capacity fade exhibited by all cells which were cycled to 4.65 V the V_{max} for formulation **2** was increased to 4.45 V after early cycling. It should be noted that for both conditions which had V_{max} increased from the initial 4.25 V that over the first several cycles at the higher voltage an increase in cycling capacity was observed. Also the current at which the cells were cycled was maintained as the voltage was increased. This resulted in a subsequent drop in the C rate. For formulation **2** the final rate was approximately C/25.

Comparison of the charge and discharge profiles for formulations **1**, **2**, and **6** are shown in Fig. 4. For all three formulations a change in the charge profile occurs as the cells age with the most distinct changes occurring at the low voltages. As the cells aged the majority of the capacity shifted to voltages above 4.1 V. A more thorough analysis of the dynamics of the charge–discharge characteristics can be accomplished by comparing the differential capacity (dQ/dV) of the different formulations as they progressed through the cycling regime. While C/10 cycling is not ideal for isolating minor features in dQ/dV plots it is sufficient to provide information on the general trends observed during cycling. The dQ/dV plots (Fig. 5) indicate that a change occurs in the storage mechanism as the cells age. Three distinct capacity regions can be defined when comparing the initial dQ/dV for the three formulations. First are capacities associated with voltages between 3.6 and 3.8 V. This region is most pronounced for formulation **6** which has a high A12 graphite component. The second region lies between 3.8 and 4.25 V and is relatively uniform for all three formulations during initial cycling. The last region lies above 4.25 V where most dQ/dV profiles show more constant (but non-zero) values. As the different formulations age, changes are most pronounced in the first two regions. In the middle region the capacity coalesces in all three to a central peak at 4.12–4.15 V.

The data in Fig. 3 clearly indicate that the various phosphazene-based anodes can achieve capacities which exceed the values anticipated for Li intercalation into the respective amounts of A12 present. The calculated values for the capacity associated with the A12 portion of each of the electrodes is shown in Table 1, with the respective percent of the total discharge capacity after 10 cycles shown after the comma in the same column. The question becomes, by what mechanisms is the energy being stored and what the limitations are on its overall applicability. As expected, for all formulations during formation the overall capacity increased as the V_{max} was increased from 3.7 V to 4.65 or 4.25 V. Post-formation the full cells cycling to 4.65 V (formulations **1**, **3**, **4** and **5**) initially displayed either stable or increasing capacity before exhibiting progressive decreases in capacity with continued cycling. Of interest is that samples (**1**, **2**, **4**, and **5**) prepared using more HMTA (0.5 g) and thus more water (1.0 mL) displayed lower capacity fade during extended cycling. Comparison of the BET and porosity measurements of these samples with previous work (data not shown) looking at similar formulations, but using less water and HMTA in the preparation steps indicates that increasing the water content resulted in a total decline in surface area (11 vs 22–26 $m^2\ g^{-1}$) and total pore volume (1.73×10^{-2} vs $2.3–3.06 \times 10^{-2}$ $cm^3\ g^{-1}$), but resulted in increased average pore diameters (63 vs 42–48 Å). This result suggests that, at least for the present formulations, that the increase in average pore diameter plays a more important role in minimizing capacity fade than the total surface area of the

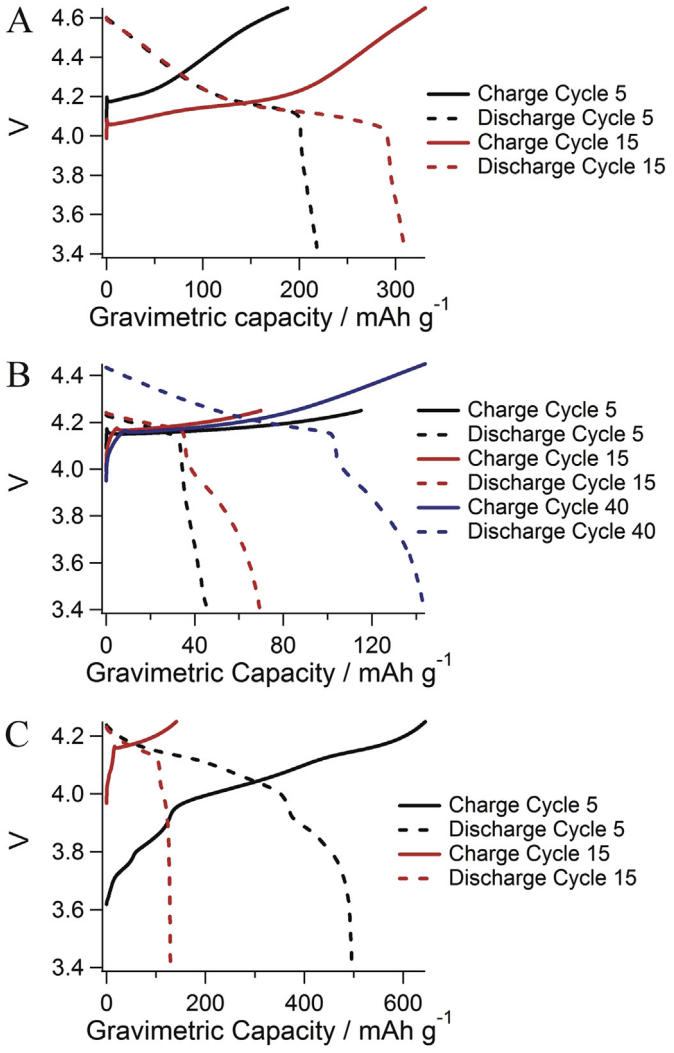

Fig. 4. Typical charge and discharge profiles for formulations **1** (A), **2** (B) and **6** (C) at the end of formation (cycle 5) and after additional cycling.

electrode. This correlation can be rationalized in two ways. First, the increased pore diameter may facilitate Li^+ transport to the interior of the electrode allowing a greater portion to remain active. Second, the increased diameter may allow greater room for the electrodeposition of micro-clusters of Li as described more fully below. For the smaller pore diameter systems such micro-clustering may induce sufficient volume change that portions of the overall electrode structure are impacted leading to either reduced pore volume for Li clusters or changes in electrical connectivity creating isolated regions within the electrode.

Similar capacity fade behavior was shown for formulation **6** cells which were initially cycled at 4.25 V followed by an increased V_{max} to 4.65 V. For this reason cycling at an intermediate voltage (4.45 V) was performed for formulation **2**. This voltage was chosen based on the early cycling results for formulation **1** which had a charge capacity of ~150 mAh g^{-1} at 4.45 V. Of the 150 mAh g^{-1} (1 mAh total), only 33 mAh g^{-1} (0.22 mAh) is attributed to the A12 with the remainder (0.78 mAh) being associated with Li deposition within the polymeric matrix. This accounts for a Li mass of 25.6 μg. Including the mass of Li into the specific capacity changes the value to 146 mAh g^{-1}. At that level, the calculated Li loading per phosphazene ring is 6.1 Li, which may have stoichiometric significance. As with formulation **6**, upon the increase in V_{max} the capacity for formulation **2** increased before plateauing for the remainder of the first 50 cycles.

Based on the idea of a hybrid anode where part of the capacity resides in a host intercalation or alloy-based material such as graphite and the remainder is associated with the distributed phosphazene network, half-cell analysis of formulation **6** (Fig. 6) was performed. Based on a comparison of the charge and discharge profiles (Fig. 4A and C) and *dQ*/*dV* (Fig. 5A and C) plots for formulations **1** and **6**, it appears that in a full cell configuration the capacity associated with the phosphazene template resides negative of the onset potential for Li insertion in graphite. As shown in Fig. 6, this is confirmed by the half-cell galvanostatic titration for formulation **6**. The initial waves correspond to Li-insertion into graphite (Region I) [33]. Negative of the initial graphite association a sloping region, indicative of a transition between reduction processes, between 0.06 and −0.02 V is observed (Region II). Within this region would occur a greater population of lithium at/near the phosphazene members under a micro-clustering process that generates the equivalent of nucleation sites for greater lithium deposition at higher voltages The voltage in Region II reaches a negative value at −0.0207 V followed by a steady, slightly positive

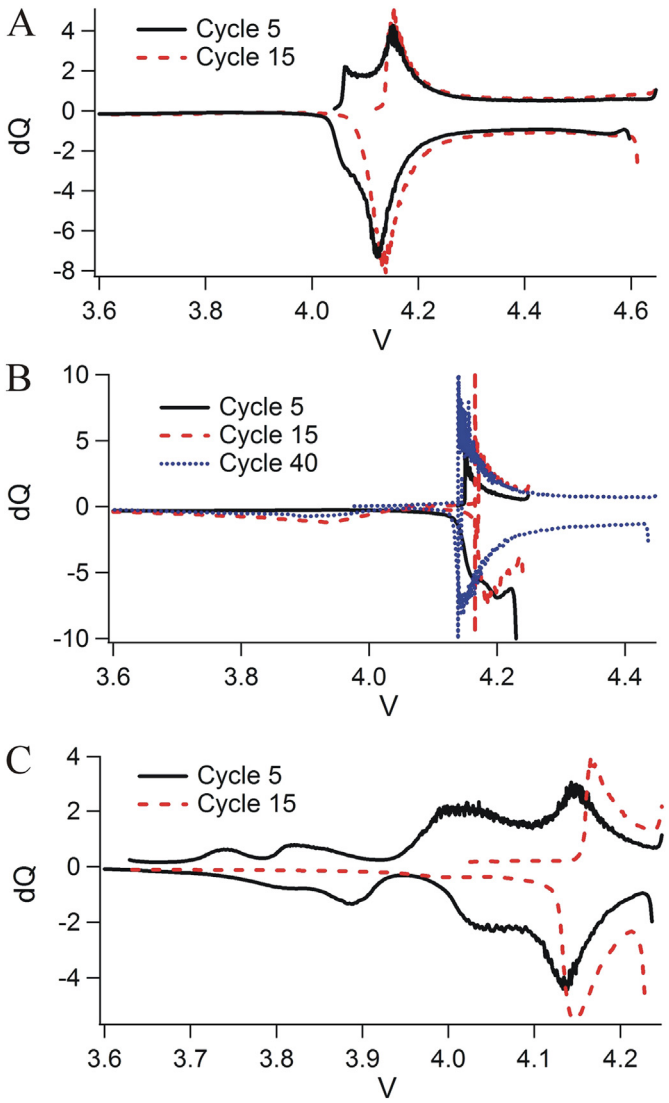

Fig. 5. Typical differential capacity (*dQ*/*dV*) plots for formulations **1** (A), **2** (B) and **6** (C) at the end of formation (cycle 5) and after additional cycling.

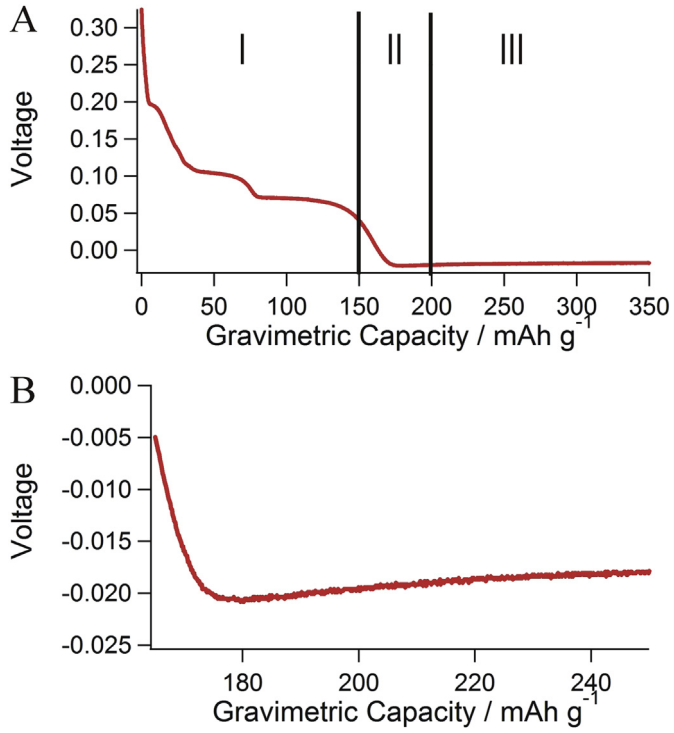

Fig. 6. Typical half-cell charge profile for formulation **6** (A). Region I corresponds to capacity associated with A12, II with initial Li nucleation and A12 and the capacity in region III is due to secondary Li deposition. Expanded view of the voltage relaxation occurring in Regions II and III following the onset of Li deposition (B).

trending plateau (Region III). Negative peaks, such as the one observed in the present case (Region II), can be indicative of a nucleation event during the electrodeposition process where the activation energy, and subsequently overpotential, needed for initial deposition determines the extent of the negative going voltage excursion [34,35]. Following the initial nucleation, the surface energy of the deposited Li becomes favorable to additional, isolated deposition of Li due to the localized regions of lower overpotential which are created. Thus, as more Li is deposited the overall energetics become more uniform as evidenced by the slight voltage rebound and plateau observed in Fig. 6B.

In many ways the electrodeposition of Li seen for the hybrid phosphazene anodes is similar to what occurs regardless of the substrate as Li electrodeposits on an electrode surface. However a few distinct differences are observed for the hybrid phosphazene anodes. During the deposition of Li on more traditional graphite anode surfaces, coulombic efficiencies as high as 98% are observed when small amounts of Li are deposited at rates between C/5 and C/10 (30 mAh g^{-1} active material) [36,37]. Beyond this early stage, and after repeated cycling at voltages at which deposition occurs, a more pronounced reduction in efficiency is observed [35,38,39]. As presented in Fig. 3C, the efficiency for formulation **2** remains near 98% for the majority of post formation cycling with a slight increase to over 99% after the increase in voltage from 4.25 to 4.45 V. Following the increased efficiency a slight decrease was observed followed by a plateau. Despite the decrease, the efficiency of the plateau remained the same as was observed prior to the increase in voltage. While the efficiency was not altered by the increased voltage, the capacity of the system increased from 71 mAh g^{-1} for the last cycle at 4.25 V to 183 mAh g^{-1} (of total electrode material) after 20 cycles at 4.45 V. The increase in capacity, while retaining the same efficiency, suggests that the environment, with respect to electrolyte interaction, of the newly deposited Li when cycling to higher voltages is similar to the environment of Li deposited at lower voltages. It is also plausible that as a greater extent of Li is deposited the overall conductivity of the electrode increases. Following the completion of cycling, BET analysis found that the total pore volume had increased to 9.16×10^{-2} cm^3 g^{-1} from 1.73×10^{-2} cm^3 g^{-1}. This suggests that as Li is deposited within the hybrid anode structure that the subsequent volume expansion leads to the increased porosity.

Formulation **1**, which had the same composition as formulation **2**, displayed similar but more pronounced increased capacities during early cycling, but at efficiencies of 96% and lower. Recall that in Fig. 6, region III is associated with bulk lithium deposition. Allowing this to proceed for extended periods of time (such as what occurs when cycling to 4.65 V) minimizes any isolation from bulk electrolyte which the phosphazene template may provide. As isolation is lost, the subsequent reaction with electrolyte leads to decreased coulombic efficiencies and loss of capacity through either the formation of thick SEI deposits or through electrical isolation of Li deposits.

The difference in efficiency between cycling to 4.65 and 4.45 V suggests that there is a limit to the quantity of Li which can be deposited within the anode structure without seeing a loss in cycling capacity and while retaining efficiencies near 98%. To determine this limitation the number of Li atoms deposited per cyclic phosphazene in the anode structure was calculated from gravimetric and charge data. If it is assumed that the A12 within formulations **1** and **2** does not remain active during extended cycling the number of Li atoms which are deposited with respect to the number of cyclic phosphazenes in the respective formulations and the total Li deposited can be determined (Fig. 7). This key assumption is based on the *dQ*/*dV* data presented in Fig. 5. As can be seen, for the lower V_{max} of 4.45 V less than 7.4 Li are deposited per MeHQCP trimer while the higher V_{max} initially has Li densities in excess of 13.6 Li per MeHQCP ring. These data suggest that there is the possibility to deposit low levels of Li within the phosphazene

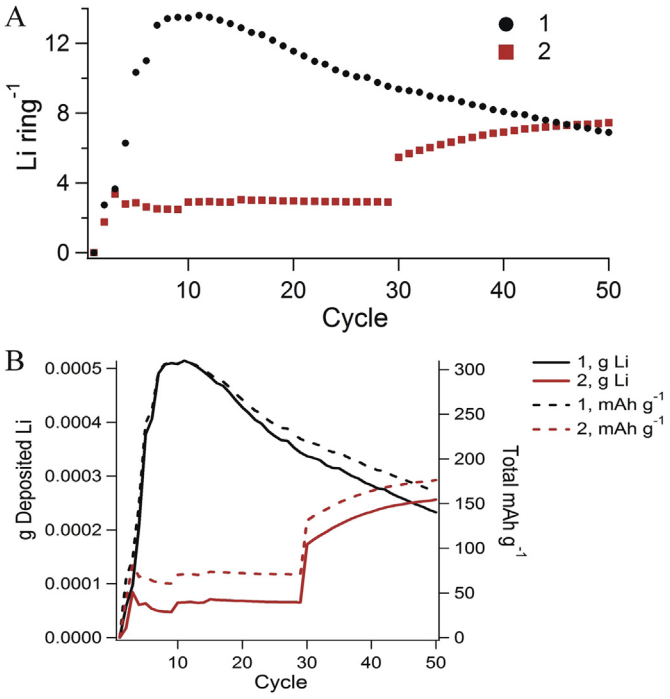

Fig. 7. (A) Calculated values for the amount of Li deposited per MeHQCP ring for formulations **1** and **2**. (B) Total g Li deposited during cycling (left) and specific capacity with Li mass included (right) for formulations **1** and **2**.

framework while retaining cycling efficiencies near 98% and that overall electrode capacity may be able to be increased by altering the molecular weight of the phosphazene used for anode formation. The data also suggest that accounting for the amount of Li deposited does not significantly change the overall capacity for the electrode systems with the variance for formulation **2** being 7 mAh g^{-1} (183 vs 176 mAh g^{-1} when accounting for Li mass).

The distinct regions in the half-cell data which are roughly delineated in Fig. 6 and the Li per ring calculations in Fig. 7 help explain the storage mechanisms and highlight some of the potential limitations and benefits associated with the proposed hybrid anodes. Foremost among considerations is the need to tightly control the V_{max} for cycling phosphazene electrodes. As expected higher voltages provide enhanced early life capacity as well as cell power, but the enhanced capacities readily fall to levels seen for cells cycled at lower voltages. This decrease is almost certainly associated with complex degradation mechanisms involving increased Li deposition, a fractional increase in Li isolation, and electrolyte oxidation/reduction. Thus, controlling V_{max} is essential for the present systems. Rate limitations also become a concern as the structure of Li deposits is strongly influenced by deposition current [34]. However, routes toward material optimization and benefits from the phosphazene systems clearly exist. Having a polymer basis allows for customization of anode attributes in terms of porosity and electronic conductivity, which have a direct bearing on rate capabilities and the manifestation of overpotentials at the anode. For example, crosslinking schemes can have a significant impact on both enhancing polymer conductivity and rheological properties. Alongside potential safety enhancement, perhaps the main benefit is that the hybrid phosphazene anodes can enable voltage specific, tailorable systems which can provide capacity in multiple regions that provide the side benefit of overcharge protection.

The systems which have been presented offer the possibility of using multiple Li storage mechanisms by allowing up to 7.4 Li to be deposited per phosphazene ring for up to 20 cycles while also intercalating Li into graphite. However, the full role and optimization of the phosphazene structures requires further investigation. Two possibilities exist for its ability to maintain enhanced efficiencies. First it may serve as a template or distributed network which facilitates deposition of Li-ions associated with the O and N components of the polymer system. In doing so the deposit is isolated from bulk electrolyte resulting in less electrolyte depletion over extended cycling. Second, it could serve as a protective shroud which minimizes the interaction of Li deposits with electrolyte. Both possibilities would decrease electrolyte decomposition at the electrodeposited Li surface and lead to the enhanced coulombic efficiency if effectively controlled. Such an understanding would allow better engineered systems to be developed with enhancements in both the overall capacity and coulombic efficiency. Additionally, the extent of safety enhancement offered by the inclusion of the phosphazene needs to be evaluated as part of future work.

4. Conclusions

Hybrid anodes consisting of graphite within a cyclic phosphazene template has been presented. The spray cast electrode films had surface areas (11–26 m^2 g^{-1}), total pore volume (1.73×10^{-2}–3.06×10^{-2} cm^3 g^{-1}) and pore diameters (42–63 Å) which were similar to the cathodes used for this study. For formulations with only 10% graphite, capacities as high as 183 mAh g^{-1} (176 mAh g^{-1} with Li mass included) have been observed after 50 cycles with efficiencies of 98%. The bulk of the capacity resides with the deposition of Li adjacent to the phosphazene moieties which minimizes the decomposition of electrolyte at the deposits. Insertion of lithium into the anode host material was found to reside in distinct regions tied directly to the choice of materials (graphite and polymer) and cell voltage. Control of V_{max} provides the possibility of cycling electrodes with no loss in capacity or efficiency over 50 cycles. Allowing extensive Li deposition reduced the efficiency and led to gradual declines in overall capacity with extended cycling. Our phosphazene polymer basis offers benefits to anode chemistry in terms of lowered flammability, customization and optimization through polymer attributes and formulation options, enhanced overcharge protection, and the polymer host acts as the binder (no need for PVDF).

Acknowledgments

The authors would like to thank Dr. Sergiy Sazhin for helpful discussion during the preparation of this manuscript. Funding was provided from Vehicle Technologies Office of the Energy Efficiency and Renewable Energy Office of the U.S. Department of Energy under the guidance of the Advanced Battery Research (ABR) program. This manuscript has been authored by Battelle Energy Alliance, LLC under Contract No. DE-AC07-05ID14517 with the U.S. Department of Energy. The United States Government retains and the publisher, by accepting the article for publication, acknowledges that the United States Government retains a nonexclusive, paid-up, irrevocable, world-wide license to publish or reproduce the published form of this manuscript, or allow others to do so, for United States Government purposes.

References

[1] S.V. Sazhin, M.K. Harrup, K.L. Gering, J. Power Sources 196 (2011) 3433–3438.
[2] B.B. Wu, F. Pei, Y. Wu, R.J. Mao, X.P. Ai, H.X. Yang, Y.L. Cao, J. Power Sources 227 (2013) 106–110.
[3] Z.C. Zhang, L.B. Hu, H.M. Wu, W. Weng, M. Koh, P.C. Redfern, L.A. Curtiss, K. Amine, Energy Environ. Sci. 6 (2013) 1806–1810.
[4] R.P. Ounn, J. Kafle, F.C. Krause, C. Hwang, B.V. Ratnakumar, M.C. Smart, B.L. Lucht, J. Electrochem. Soc. 159 (2012) A2100–A2108.
[5] M.Q. Xu, L. Zhou, L.S. Hao, L.D. Xing, W.S. Li, B.L. Lucht, J. Power Sources 196 (2011) 6794–6801.
[6] P. Ping, Q.S. Wang, J.H. Sun, X. Xia, J.R. Dahn, J. Electrochem. Soc. 159 (2012) A1467–A1473.
[7] X. Xia, P. Ping, J.R. Dahn, J. Electrochem. Soc. 159 (2012) A1460–A1466.
[8] M.K. Harrup, K.L. Gering, H.W. Rollins, S.V. Sazhin, M.T. Bension, D.K. Jamison, C.J. Michelbacher, T.A. Luther, ECS Trans. 41 (2012) 13–25.
[9] D.P. Abraham, E.P. Roth, R. Kostecki, K. McCarthy, S. MacLaren, D.H. Doughty, J. Power Sources 161 (2006) 648–657.
[10] M.N. Richard, J.R. Dahn, J. Electrochem. Soc. 146 (1999) 2068–2077.
[11] M.N. Richard, J.R. Dahn, J. Electrochem. Soc. 146 (1999) 2078–2084.
[12] S.T. Fei, H.R. Allcock, J. Power Sources 195 (2010) 2082–2088.
[13] H.R. Allcock, E.C. Kellam, R.V. Morford, Solid State Ionics 143 (2001) 297–308.
[14] H.R. Allcock, R. Prange, T.J. Hartle, Macromolecules 34 (2001) 5463–5470.
[15] L. Gao, D.D. Macdonald, M. Urquidi-Macdonald, D.L. Olmeijer, H.R. Allcock, Electrochim. Acta 47 (2002) 3863–3872.
[16] H.R. Allcock, E.C. Kellam, Solid State Ionics 156 (2003) 401–414.
[17] G. Nazri, D.M. MacArthur, J.F. Ogara, Chem. Mater. 1 (1989) 370–374.
[18] H.W. Rollins, M.K. Harrup, E.J. Dufek, D.K. Jamison, S.V. Sazhin, K.L. Gering, D.L. Daubaras, J. Power Sources 263 (2014) 66–74.
[19] T.A. Luther, F.F. Stewart, J.L. Budzien, R.A. LaViolette, W.F. Bauer, M.K. Harrup, C.W. Allen, A. Elayan, J. Phys. Chem. B 107 (2003) 3168–3176.
[20] D.K. Lee, H.R. Allcock, Solid State Ionics 181 (2010) 1721–1726.
[21] G.X. Xu, B.T. Yu, Q. Lu, Macromol. Mater. Eng. 290 (2005) 996–1000.
[22] G.X. Xu, Q. Lu, B.T. Yu, L. Wen, Solid State Ionics 177 (2006) 305–309.
[23] M.T. Benson, M.K. Harrup, K.L. Gering, Comp. Theor. Chem. 1005 (2013) 25–34.
[24] J.L.M. Abboud, R. Notario, Pure Appl. Chem. 71 (1999) 645–718.
[25] R. Mukherjee, A.V. Thomas, D. Datta, E. Singh, J. Li, O. Eksik, V.B. Shenoy, N. Koratkar, Nat. Commun. 5 (2014), http://dx.doi.org/10.1038/ncomms4710.
[26] K.L. Gering, F.F. Stewart, A.D. Wilson, M.L. Stone, United States Patent Application 20,130,196,223, 2013.
[27] F.F. Stewart, M.K. Harrup, J. Appl. Polym. Sci. 72 (1999) 1085–1090.
[28] T.A. Luther, F.F. Stewart, R.P. Lash, J.E. Wey, M.K. Harrup, J. Appl. Polym. Sci. 82 (2001) 3439–3446.
[29] S. Brunauer, P.H. Emmett, E. Teller, J. Am. Chem. Soc. 60 (1938) 309–319.
[30] B.C. Lippens, J.H. Deboer, J. Catal. 4 (1965) 319.

[31] K. Zaghib, A. Mauger, F. Gendron, C.M. Julien, Solid State Ionics 179 (2008) 16–23.
[32] L.-F. Cui, L. Hu, J.W. Choi, Y. Cui, ACS Nano 4 (2010) 3671–3678.
[33] M.D. Levi, D. Aurbach, J. Phys. Chem. B 101 (1997) 4630–4640.
[34] F. Sagane, K. Ikeda, K. Okita, H. Sano, H. Sakaebe, Y. Iriyama, J. Power Sources 233 (2013) 34–42.
[35] D. Pletcher, J.F. Rohan, A.G. Ritchie, Electrochim. Acta 39 (1994) 2015–2023.
[36] L.E. Downie, L.J. Krause, J.C. Burns, L.D. Jensen, V.L. Chevrier, J.R. Dahn, J. Electrochem. Soc. 160 (2013) A588–A594.
[37] W.Q. Lu, C.M. Lopez, N. Liu, J.T. Vaughey, A. Jansen, D.W. Dees, J. Electrochem. Soc. 159 (2012) A566–A570.
[38] S.V. Sazhin, M.Y. Khimchenko, Y.N. Tritenichenko, W. Roh, H.Y. Kang, J. Power Sources 66 (1997) 141–145.
[39] E. Eweka, J.R. Owen, A. Ritchie, J. Power Sources 65 (1997) 247–251.